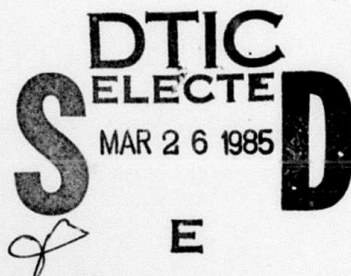


Collective Effects in the

Free Electron Laser (FEL)

P. Sprangle, C. M. Tang and C. W. Roberson\*

Plasma Theory Branch  
Plasma Physics Division  
Naval Research Laboratory  
Washington, DC 20375-5000



- I. Introduction
- II. Linear Theory of the FEL, FEL dispersion relation, high gain Compton regime, Raman regime, low gain Compton regime, intrinsic laser efficiency and beam thermal limitations.
- III. Nonlinear Theory of the FEL, wave equations, nonlinear driving currents, particle dynamics, coupled pendulum and wave equations, numerical results in the Raman regime, efficiency enhancement.

This document has been approved  
for public release and sale; its  
distribution is unlimited.

ABSTRACT

With intense relativistic electron beams, such as generated by induction linear accelerators, pulsed transmission line accelerators or high current RF linacs, collective effects can play an important role in the FEL process. High gain FELs are said to operate in the Raman regime when collective effects dominate the usual ponderomotive effects. Collective effects may also play an important role in low gain FELs when the beam current is sufficiently high. In this paper the linear and nonlinear dynamics of the FEL mechanisms, including space charge effects, is analyzed. The various collective and noncollective operating regimes are discussed.

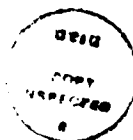
\* Present address: Office of Naval Research, Arlington, VA.

## I. Introduction

Although the first ideas for the free electron laser have been known since the original article by Motz [1] in 1951 and the successful experiments by Phillips [2] in 1960, it is the recent work that has made the free electron laser a serious candidate for a powerful new radiation source. In fact the free electron laser has become the conceptual alternative for virtually every radiation source from the microwave to the ultraviolet [3]. This can be understood by examining Fig. 1, where the power vs. wavelength of high power coherent radiation sources is plotted. These sources include gas and solid state lasers, conventional microwave tubes and gyrotrons. The potential operating range not only covers the entire wavelength range, but maximum power levels are comparable with the other conventional high power coherent radiation sources.

Existing accelerator technology together with the characteristics of the FEL interaction mechanism divide FELs into distinct categories [4-7]. These categories are distinguished primarily by the type and characteristics of the electron beam source.

Free electron lasers based on such beams as RF linacs, microtrons or storage rings can be expected to operate in what is referred to as the "Compton" regime [4-11]. Such beams are generally of high energy, low current and high quality (low emittance). The Compton regime is one in which the interaction physics is primarily governed by single-particle effects; collective or space charge effects can usually be neglected. Typically in this regime the radiation gain is low, thus, practical sources operating in this regime would necessarily function as oscillators where high gain is not a crucial requirement. In the absence of efficiency enhancement techniques, the operating efficiencies are generally low, (e.g., a fraction of a percent).



For

<input checked="" type="checkbox"/>
<input type="checkbox"/>
<input type="checkbox"/>

on/

ity Codes

and/or

Special

Dist

Special

A-1

Since the beam energy and quality is generally high, FELs in this regime can operate in the optical regime or beyond.

Free electron lasers based on intense relativistic electron beams (IREB) such as, pulse line accelerators [12-15] or induction linac accelerators [16-18], operate in the "Raman" or "collective" regime [4-7,19,20]. Here collective effects play an important role in determining such characteristics as the radiation growth rate, interaction efficiency, etc. The FEL operating wavelength, however, remains well-approximated by the usual expression appropriate for the Compton regime. Numerous FEL experiments have been performed with pulse line generated beams. These beams are produced from plasma induced field emission diodes, and have a relatively flat voltage and current pulse lasting for a few tens of nanoseconds. Typically they are in the MeV energy range and carry kiloamperes of current. The low energy and quality of these beams limit their operation in FELs to the millimeter regime. Since the beam current is high, the radiation gain (or spatial growth rate) can be large enough to make operation as an FEL amplifier possible.

There is a third operating regime which has features that are common to both the Compton and Raman regimes. Here the wiggler field is strong enough so that the ponderomotive force on the electrons completely dominates the space charge forces and the radiation growth rate is large. We will refer to this regime as the "High-Gain Compton" [4,5]. Free electron lasers using storage ring generated electron beams may operate in this regime to produce x-rays [21-23].

## II Linear Theory of the Free Electron Laser

The essential feature of the FEL mechanism is that the electrons undergo axial bunching in the combined wiggler and radiation fields. In this section

we will discuss the details of the FEL mechanism in the linear or small signal regime. The nonlinear dynamics will be discussed in section III.

The physical model consists of a relativistic electron beam of arbitrary intensity entering and propagating through a static helically polarized wiggler field. Only spatial variations along the  $z$  axis will be considered for the electron beam, wiggler field, radiation fields and space charge waves. Figure 2 shows the basic components of a FEL employing a linearly polarized wiggler field. In both the linear and nonlinear analysis contained in this paper a helically polarized wiggler field is used. Using our model we obtain expressions for the radiation field, the perturbed charge density and ponderomotive potential. This set of coupled equations fully describe the FEL interaction. A dispersion relation, in the high gain regimes, is derived which shows explicitly the coupling of the electromagnetic and space charge waves by the wiggler field.

For cold electron beams, we find two regimes where the radiation grows exponentially. In the collective, or Raman regime, the contribution to the perturbed beam density (and hence radiation output) due to the self consistent space charge potential is greater than that due to the ponderomotive potential. In the high gain Compton regime (strong wiggler and/or tenuous beam limit) the contribution to the perturbed beam density from the ponderomotive wave dominates that due to the self consistent space charge potential. This regime can be obtained by increasing the wiggler amplitude or reducing the beam density. The interaction in the high gain Compton regime is not a collective one as it is in the Raman regime.

We also obtain the small signal radiation gain with space charge effects in the low gain Compton regime. This result is obtained by taking Laplace transforms of the three equations for the ponderomotive potential, density

perturbation and radiation field. The low gain Compton mechanism is a result of constructive interference of modes rather than exponential growth of an instability.

The helically polarized, static, periodic, magnetic wiggler is taken to have the form

$$\underline{B}_w(z) = B_w (\cos(k_w z) \hat{e}_x + \sin(k_w z) \hat{e}_y), \quad (1)$$

where  $B_w$  is constant,  $k_w = 2\pi/\lambda_w$ , and  $\lambda_w$  is the wiggler wavelength. This form is sufficient for particles near the axis, i.e.,  $k_w r_b \ll 1$  where  $r_b$  is the beam radius. A more realistic representation can be found in Refs. 8 and 9. The vector potential associated with this wiggler field is

$$\underline{A}_w = A_w (e^{ik_w z} \hat{e}_- + e^{-ik_w z} \hat{e}_+), \quad (2)$$

where  $A_w = B_w/k_w$ , and  $\hat{e}_\pm = (\hat{e}_x \pm i\hat{e}_y)/2$ . Electrons streaming axially in the presence of the wiggler field (2) and radiation field produce a driving current which can stimulate (amplify) the imposed radiation field. The radiation field, which we will represent by its vector potential  $\underline{A}_R(z,t)$ , evolves according to the wave equation

$$\left( \frac{\partial^2}{\partial z^2} - \frac{1}{c^2} \frac{\partial^2}{\partial t^2} \right) \underline{A}_R = - \frac{4\pi}{c} \underline{J}_1, \quad (3)$$

where  $\underline{J}_1$  is the ponderomotive induced transverse driving current. In a form similar to the representation of the wiggler field (2) we represent the stimulated radiation by

$$\underline{A}_R(z,t) = A_R(e^{i\phi(z,t)}\hat{e}_+ + e^{-i\phi(z,t)}\hat{e}_-), \quad (4)$$

where  $A_R$  is the amplitude,  $\phi(z,t) = kz - \omega t$  is the phase,  $k$  is the complex wavenumber and  $\omega$  is the real frequency. The wiggler induced transverse driving current is given by

$$\underline{J}_\perp(z,t) = -|e|(\delta n \underline{v}_w + n_0 \underline{v}_R) + (\text{nonresonant terms}), \quad (5)$$

where  $\delta n$  is the perturbed beam density,  $\underline{v}_w$  is the transverse velocity induced by the wiggler field,  $n_0$  is the ambient beam density and  $\underline{v}_R$  is the transverse velocity induced by the radiation field. The transverse wiggler and radiation velocities are obtained by the relativistic force equation for the particles,

$$d\underline{P}/dt = -|e|(\underline{E} + (\underline{P} \times \underline{B})/\gamma m_0 c), \quad (6)$$

where  $\underline{P} = \gamma m_0 \underline{v}$ ,  $\gamma = (1 + \underline{P} \cdot \underline{P}/m_0^2 c^2)^{1/2} = (1 - \underline{v} \cdot \underline{v}/c^2)^{-1/2}$  is the total relativistic mass factor. The fields  $\underline{E}$  and  $\underline{B}$  are

$$\underline{E}(z,t) = -\frac{\partial \phi}{\partial z} \hat{e}_z - \frac{1}{c} \frac{\partial \underline{A}_R}{\partial t} \quad (7a)$$

$$\underline{B}(z,t) = \frac{\partial}{\partial z} (\hat{e}_z \times (\underline{A}_w + \underline{A}_R)), \quad (7b)$$

where  $\phi$  is the space charge potential associated with the perturbed density,  $\delta n$ , and is given by

$$\frac{\partial^2 \phi}{\partial z^2} = 4\pi |e| \delta n. \quad (7c)$$

From (6), conservation of canonical transverse momentum, i.e.,

$\gamma m_0 \underline{v} - |e| \underline{A}_w / c = \text{constant}$ , implies that

$$\underline{v}_w = \frac{|e|}{\gamma m_0 c} \underline{A}_w \quad (8a)$$

and

$$\underline{v}_R = \frac{|e|}{\gamma m_0 c} \underline{A}_R. \quad (8b)$$

Substituting (5) together with (8) into (3) yields

$$\left( \frac{\partial^2}{\partial z^2} - \frac{1}{c^2} \frac{\partial^2}{\partial t^2} - \frac{\omega_p^2}{\gamma_0 c^2} \right) \underline{A}_R = \frac{4\pi |e|^2 \delta n}{\gamma_0 m_0 c^2} \underline{A}_w. \quad (9)$$

From Eq. (9), we see that the radiation field,  $\underline{A}_R$ , is driven by the wiggler field,  $\underline{A}_w$ , and the beam density perturbation,  $\delta n$ . The perturbed beam density must now be determined self consistently. From charge conservation, the perturbed beam density is given by

$$\frac{\partial \delta n}{\partial t} = \frac{1}{|e|} \frac{\partial \delta J_z}{\partial z}, \quad (10)$$

where  $\delta J_z$  is the perturbed axial beam current given by

$$\delta J_z(z, t) = - |e| (n_0 \delta v_z + \delta n v_{z0}). \quad (11)$$

In Eq. (11),  $\delta v_z$  and  $v_{z0}$  are the perturbed and unperturbed axial electron velocities. Combining (10) and (11) yields the following expression for the perturbed density,

$$\frac{d\delta n}{dt} = -n_0 \frac{\partial \delta v_z}{\partial z}. \quad (12)$$

Taking the axial component of the force equation, Eq. (6), and using the relation  $dy/dt = -|e|(\underline{v} \cdot \underline{E})/m_0 c^2$  we find that

$$\frac{dv_z}{dt} = -\frac{|e|}{\gamma m_0} \left\{ -\frac{\partial \phi}{\partial z} + \frac{(\underline{v} \times \underline{B}) \cdot \hat{e}_z}{c} - \frac{v_z (\underline{v} \cdot \underline{E})}{c^2} \right\}. \quad (13)$$

Linearizing (13) by keeping terms to first order in the radiation field yields

$$\frac{d\delta v_z}{dt} = -\frac{|e|}{\gamma_0 m_0} \left\{ \gamma_z^{-2} \frac{\partial \phi(z,t)}{\partial z} + \left( \frac{\partial}{\partial z} + \frac{v_{z0}}{c^2} \frac{\partial}{\partial t} \right) \phi_p(z,t) \right\}. \quad (14)$$

In Eq. (14), the  $\gamma_z^{-2}$  relativistic reduction in the space charge field comes from combining the terms  $\partial \phi / \partial z$  and  $-(v_{z0}/c)^2 \partial \phi / \partial z$  in Eq. (13) where  $\gamma_z = (1 - v_z^2/c^2)^{-1/2}$ . The relativistic factors  $\gamma$  and  $\gamma_z$  are related by  $\gamma_0 = \gamma_z \{1 + (|e|A_w/m_0 c^2)^2\}^{1/2}$ . The axial force terms due to  $\underline{v} \times \underline{B}/c$  and  $v_{z0}(\underline{v} \cdot \underline{E})/c^2$  can be written in terms of an effective potential called the ponderomotive potential,  $\phi_p$ , where

$$\phi_p(z,t) = \frac{-|e| \frac{\underline{A}_w \cdot \underline{A}_R}{2}}{\gamma_0 m_0 c^2} = \frac{-|e| \frac{A_w A_R}{2}}{2\gamma_0 m_0 c^2} e^{i((k+k_w)z - \omega t)} + c.c.. \quad (15)$$

We see from Eq. (14) that the beam velocity and, hence, density is driven by both the ponderomotive and space charge potential waves. The ponderomotive wave in turn is proportional to the wiggler and radiation field amplitudes. Taking the convective time derivative of both sides of (12) and employing (14) yields

$$\frac{d^2 \delta n}{dt^2} = \frac{-|e|n_0}{\gamma_0 m_0} \left\{ \frac{1}{\gamma_z^2} \frac{\partial^2 \phi(z,t)}{\partial z^2} + \frac{\partial}{\partial z} \left( \frac{\partial}{\partial z} + \frac{v_{z0}}{c^2} \frac{\partial}{\partial t} \right) \phi_p(z,t) \right\}. \quad (16)$$

Substituting (7c) into (16) and using  $\partial^2 \phi / \partial z^2 = 4\pi |e| \delta n$  we obtain

$$\frac{d^2 \delta n}{dt^2} + \frac{\omega_p^2}{\gamma_o \gamma_z^2} \delta n = \frac{-|e| n_o}{\gamma_o m_o} \frac{\partial}{\partial z} \left( \frac{\partial}{\partial z} + \frac{v_{zo}}{c} \frac{\partial}{\partial t} \right) \phi_p(z, t). \quad (17)$$

Equation (17) shows that the perturbed charge density is driven by the ponderomotive potential wave. Equations (9) and (17) together with (15) form a set of coupled relations for the radiation field and perturbed charge density. The beam density perturbation is driven by the ponderomotive wave, which is proportional to the radiation field. The radiation field in turn is driven by both the ponderomotive wave and wiggler field. The coupling in these equations, under appropriate conditions, can lead to radiation growth.

#### FEL Dispersion Relation

The phase of the ponderomotive wave is  $(k + k_w)z - \omega t$ . From Eq. (17) we see that the perturbed density should have a similar dependence in the time asymptotic limit, hence we write

$$\delta n(z, t) = \tilde{\delta n}(k, \omega) e^{i((k + k_w)z - \omega t)} + c.c. \quad (18)$$

Using (18) together with (15), Eq. (17) becomes

$$\begin{aligned} & \left[ (\omega - v_{zo}(k + k_w))^2 - \frac{\omega_p^2}{\gamma_o \gamma_z^2} \right] \tilde{\delta n} \\ &= \frac{\omega_p^2}{8\pi \gamma_o^2} \frac{A_w A_R}{m_o c^2} (k + k_w) \left( k + k_w - \frac{v_{zo} \omega}{c} \right). \end{aligned} \quad (19)$$

Equations (9) and (17) can be used in the high gain regime to obtain a dispersion relation for the radiation field. In this section transient terms

associated with the initial value solution of (9) and (19) will be neglected. Substituting (18) together with the representations for  $\underline{A}_w(z)$  and  $\underline{A}_R(z,t)$  given in (2) and (4), into (9) gives

$$\left(k^2 - \frac{\omega^2}{c^2} + \frac{\omega_b^2}{\gamma_o^2 c^2}\right) A_R = \frac{-4\pi|e|^2}{\gamma_o m_o c^2} \delta\tilde{n} A_w. \quad (20)$$

Eliminating  $\delta\tilde{n}$  and  $\tilde{A}_R$  from (19) and (20) yields the following dispersion relation

$$\begin{aligned} & \left[\omega^2 - c^2 k^2 - \omega_b^2/\gamma_o\right] \left[\left(\omega - v_{zo}(k+k_w)\right)^2 - \omega_b^2/\gamma_o\gamma_z^2\right] \\ & = \frac{\omega_b^2}{\gamma_o^2} \beta_w^2 c^2 k k_w, \end{aligned} \quad (21)$$

where  $v_w = c\beta_w = |e|A_w/(\gamma_o m_o c)$  is the magnitude of the electron wiggler velocity. In obtaining the final dispersion relation in (21) we used the approximations  $k \approx (1 + \beta_z)\gamma_z^2 k_w \gg k_w$  and  $\omega \approx ck$  to simplify the terms on the right hand side of (19), i.e.,

$$(k + k_w) \left(k + k_w - \frac{v_{zo}\omega}{c^2}\right) \approx 2 k k_w.$$

In (21) the first term in brackets represents the uncoupled electromagnetic mode while the second bracketed term represents the two uncoupled beam space charge modes having an effective wavenumber  $k + k_w$ . The wiggler field provides for the coupling between the electromagnetic and space charge modes. Since we will be primarily concerned with the forward travelling radiation field we can approximate the electromagnetic mode, in (21) by

$$\omega^2 - c^2 k^2 - \omega_b^2 / \gamma_0 \approx 2 \omega (\omega - (c^2 k^2 + \omega_b^2 / \gamma_0)^{1/2}). \quad (22)$$

Using (22) the FEL dispersion relation becomes

$$\begin{aligned} & \{k - (\omega^2/c^2 - \omega_b^2/\gamma_0 c^2)^{1/2}\} \{(\omega/v_{zo} - k_w)^2 - \frac{\omega_b^2}{v_{zo}^2 \gamma_0 \gamma_z^2}\} \\ &= - \frac{\omega_b^2/c^2}{2\gamma_0} \beta_w^2 \frac{k_w}{\beta_{zo}^2}. \end{aligned} \quad (23)$$

The dispersion relation in (23) may now be re-cast into the form

$$(k - k_{em})(k - k_-)(k - k_+) = -\alpha^2, \quad (24)$$

where  $\alpha^2 = \frac{\omega_b^2/c^2}{2\gamma_0} \beta_w^2 \frac{k_w}{\beta_{zo}^2}$  is the coupling coefficient,

$$k_{em} = (\omega^2 - \omega_b^2/\gamma_0)^{1/2}/c, \quad (25a)$$

is the electromagnetic mode wavenumber and

$$k_{\pm} = \{\omega - v_{zo} k_w \mp \omega_b/(\gamma_z \sqrt{\gamma_0})\}/v_{zo}, \quad (25b)$$

is the wavenumber of the positive and negative energy beam space charge modes respectively. We can now distinguish two operating regimes of the FEL mechanism, often referred to as the high gain noncollective (strong wiggler) and Raman regimes.

### High Gain Compton Regime

In this regime the forces on the beam electrons due to the ponderomotive wave dominates that due to the collective space charge effects. This can also be referred to as the strong wiggler field limit or tenuous beam limit and is a noncollective process. In this limit the dispersion relation (23) reduces to

$$(k - k_{em}) \{k - (\omega/v_{zo} - k_w)\}^2 = -\alpha^2, \quad (26)$$

where the space charge term which comes about from the self consistent scalar potential, i.e.,  $\omega_b/(v_{oz} \gamma_z \sqrt{\gamma_0})$  has been neglected. From the character of the dispersion relation in (26) it is clear that this regime involves the coupling of an electromagnetic mode with the ponderomotive wave. The maximum spatial growth rate occurs when  $k_{em}$  is equal to  $(\omega - v_{zo} k_w)/v_{zo}$  and is given by

$$\Gamma = \frac{\sqrt{3}}{2} \left( \frac{\beta_w^2}{2} \frac{\omega_b^2 k_w}{\gamma_0^2 c^2} \right)^{1/3}. \quad (27)$$

In obtaining (27) we used the approximations,  $\omega \approx ck$  and  $\beta_{oz} \approx 1$ . The dispersion relation in (26) was obtained by neglecting the space charge term, this implies the following inequality between the wiggler field amplitude and beam density

$$\beta_w \gg \beta_{crit} = \left( \frac{2\omega_b}{c \gamma_0^{1/2} k_w \gamma_z^3} \right)^{1/2}. \quad (28)$$

At the maximum growth rate the frequency of the electromagnetic wave is  $\omega = (1 + \beta_{zo}^2) \gamma_z^2 v_{zo} k_w \approx 2\gamma_z^2 ck_w$ , where we have neglected  $\omega_b/\sqrt{\gamma_0}$  compared to  $\omega$ .

## Raman Regime

The Raman regime involves a coupling between the forward travelling electromagnetic mode and the negative energy beam space charge mode. In this regime the beam plasma frequency is sufficiently high that the coupling between the electromagnetic wave and the two beam waves, i.e., negative and positive energy modes, can be considered independently. The dispersion relation describing the interaction between the negative energy beam wave and electromagnetic wave is obtained from (24). Here, the effect of the positive energy beam mode on the coupling is weak and therefore  $k - k_+$  can be replaced by  $(k_- - k_+) = 2\omega_b/(\gamma_z v_{zo} \sqrt{\gamma_o})$  in (24). The resulting dispersion relation is

$$(k - k_{em})(k - k_-) = - \frac{\alpha^2 \gamma_z \sqrt{\gamma_o} v_{zo}}{2\omega_b}. \quad (29)$$

The maximum Raman growth rate occurs when  $k_{em} = k_-$  and is

$$\Gamma = \beta_w \left( \frac{\omega_b \gamma_z k_w}{4\sqrt{\gamma_o} c} \right)^{1/2}. \quad (30)$$

The coupling with the positive energy beam wave is indeed weak, permitting the replacement of  $k - k_+$  by  $(k_- - k_+)$  if

$$\beta_w \ll \left( \frac{2\omega_b}{c\sqrt{\gamma_o} k_w \gamma_z^3} \right)^{1/2}. \quad (31)$$

Note that (31) is the reverse inequality as in the High Gain Compton Regime given by (28).

Another method of separating the Raman regime from the high gain Compton regime is that

$$\omega_p \gg \omega_{p,crit} = \frac{1}{2} c \beta_w^2 \gamma_o^{1/2} k_w \gamma_z^3$$

in the Raman regime, while  $\omega_p < \omega_{p,crit}$  in the Compton regime.

### Low Gain Compton Regime

In this section we will simply state the low gain expression for what is usually referred to as the Compton regime. In this limit the space charge potential usually plays a small role. It differs from the high gain Compton regime by the role of the initial conditions. In the previous section we took Fourier transforms to obtain the FEL dispersion relation in (21). The Raman and high gain Compton regimes exist in the long time asymptotic limit and their characteristics are independent of the initial conditions. To obtain the gain in the present regime we take Laplace transforms of Eqs. (9) and (17). The low gain Compton regime gain with space charge effects [24] can be shown to be given by

$$G(z) = \frac{-\beta_w^2}{8} \frac{\omega_b^2}{\gamma_o^2 c^2} k_w z^3 \frac{\partial}{\partial \theta} \left( 1 + k_b^2 z^2 \frac{\partial^2}{\partial \theta^2} \right) \left( \frac{\sin \theta}{\theta} \right)^2, \quad (32)$$

where  $k_b = (\omega_b / \gamma_{zo} c) / (24 \gamma_o)^{1/2}$ ,  $|G(z)| \ll 1$ ,  $\theta = \Delta k z / 2$  and  $\Delta k = k + k_w - \omega / v_{zo}$ . In the absence of space charge effects, i.e.,  $k_b^2 z^2 \ll 1$ , the small signal gain in (32) reduces to the usual expression [4-10,25]. Since the function  $\partial(\sin \theta / \theta)^2 / \partial \theta$  has a minimum value of 0.54 when  $\theta = 1.3$ , the maximum gain is given by

$$G(z)_{\max} \approx \frac{\beta_w^2 \omega_b^2}{\gamma_o^2 c^2} k_w z^3, \quad (33)$$

where  $z = 2.6 / \Delta k = 2.6 / (k + k_w - \omega / v_{zo})$ .

### Intrinsic Laser Efficiency and Beam Thermal Limitations

Estimates of the laser efficiency for monoenergetic injected electron beams can be obtained using simple trapping arguments [5,26]. In the FEL mechanism electron trapping in the longitudinal wave, i.e., ponderomotive and space charge wave, is the saturation mechanism when the injected electron beam is monoenergetic in the longitudinal direction. The axial phase velocity of the longitudinal wave is

$$v_{ph} = \omega / (\text{Re}(k) + k_w), \quad (34)$$

where  $\text{Re}(k)$  is determined from the dispersion relation. In the linear development of the laser radiation the injected axial beam velocity is slightly greater than the phase velocity,  $v_{zo} = v_{ph} + \Delta v$  where  $v_{ph} \gg \Delta v > 0$  and  $\Delta v$  depends upon the particular FEL regime under consideration. Since radiation growth occurs when  $\Delta v \geq 0$ , the phase velocity of the longitudinal wave must be slightly less than the initial axial electron velocity. The radiation amplitude increases at the expense of the electron's kinetic energy until the electrons become deeply trapped in the longitudinal wave. At this point the radiation field reaches its maximum amplitude and the average axial electron velocity is approximately given by  $v_z \Big|_{\text{sat}} = v_{ph} - \Delta v$ . At saturation the average axial electron velocity has decreased by approximately  $2\Delta v$ . The decrease in the electron beam energy can be directly equated to the increase in radiation energy. For highly relativistic electron beams the decrease in the average electron kinetic energy is  $\Delta \epsilon = 2\gamma_o \gamma_{zo}^2 m_o v_{zo} \Delta v$  and hence the radiation efficiency is

$$\eta = \frac{\Delta \epsilon}{(\gamma_o - 1)m_o c^2} \approx 2\gamma_{zo}^2 \Delta v / c. \quad (35)$$

The longitudinal waves "see" the beam as monoenergetic if the beam's axial velocity spread is small compared to  $\Delta v$ . Since the fractional beam's axial energy spread is  $E_{th}/E_o = \gamma_{zo}^2 v_{th}/c$ , the monoenergetic beam approximation requires that

$$\frac{E_{th}}{E_o} \ll \eta. \quad (36)$$

To obtain the intrinsic efficiency,  $\eta$ , at the maximum growth rate, in the high gain Compton regime we solve (26) for  $\text{Re}(k)$ . We find

$$\text{Re}(k) = \omega/v_{oz} - k_w + \left\{ \frac{\omega_b \beta_w}{\sqrt{\gamma_o} c k_w} \right\}^{2/3} \frac{k_w}{2^{4/3}}. \quad (37)$$

Using (37) to solve for  $\Delta v = v_{zo} - v_{ph}$ , Eq. (35) yields the following expression for the intrinsic efficiency in the high gain Compton regime

$$\eta = \left\{ \frac{\omega_b \beta_w}{4\sqrt{\gamma_o} c k_w} \right\}^{2/3}. \quad (38)$$

Following the same procedure, the intrinsic efficiency in the Raman regime is

$$\eta = \frac{\omega_b / \sqrt{\gamma_o}}{\gamma_z c k_w}, \quad (39)$$

and in the low gain Compton regime is given by

$$\eta = \lambda_w / (2L) \quad (40)$$

where  $L$  is the interaction length. Table I lists the various expressions for the spatial growth rates, or gain and the corresponding intrinsic power

efficiencies for the various FEL operating regimes discussed. Operating the FEL at shorter wavelengths by increasing the beam energy or decreasing the wiggler period results in lower efficiencies and more stringent requirements on the beam energy spread. One can attempt to compensate for this by increasing the beam density, however this is usually associated with an increase in beam temperature.

### III. Nonlinear Theory of the Free Electron Laser

In this section the physical model is identical to the one used for the linear treatment of the FEL, except here the wiggler field is spatially tapered [26-28]. Here again only spatial variations along the  $z$  axis will be considered for the electron beam, wiggler, radiation and space charge fields.

The variable amplitude and period wiggler magnetic field can be expressed in terms of the vector potential

$$\underline{A}_w(z) = A_w(z) \left\{ \cos\left(\int_0^z k_w(z') dz'\right) \hat{e}_x + \sin\left(\int_0^z k_w(z') dz'\right) \hat{e}_y \right\}, \quad (41)$$

where the amplitude  $A_w(z)$  and wavenumber  $k_w(z)$  are known and slowly varying functions of  $z$ . The potential field in (41) is a good approximation to a right-handed polarized helical magnetic field near the  $z$ -axis, i.e., when  $k_w r_b \ll 1$ , where  $r_b$  is the beam radius. The wiggler magnetic field associated with (41) is given by

$$\underline{B}_w(z) = B_w(z) \left\{ \cos\left(\int_0^z k_w(z') dz' + a(z)\right) \hat{e}_x + \sin\left(\int_0^z k_w(z') dz' + a(z)\right) \hat{e}_y \right\}, \quad (42)$$

where  $B_w(z) = - \{ (k_w(z) A_w(z))^2 + (\partial A_w(z) / \partial z)^2 \}^{1/2}$ , and  $a(z) = - \tan^{-1} \{ (\partial A_w(z) / \partial z) / (k_w(z) A_w(z)) \}$ , are slowly varying functions of  $z$ . The

period of the magnetic field is  $\lambda_w(z) = 2\pi/(k_w(z) + \partial a/\partial z) \approx 2\pi/k_w(z)$ .

The scattered electromagnetic and electrostatic fields in terms of the vector potential  $\underline{A}_R(z,t)$  and scalar potential  $\phi(z,t)$  are taken to be

$$\underline{A}_R(z,t) = A_R(z) \{ \cos \phi(z,t) \hat{e}_x - \sin \phi(z,t) \hat{e}_y \}, \quad (43a)$$

$$\phi(z,t) = \phi_1(z) \cos \phi_p(z,t) + \phi_2(z) \sin \phi_p(z,t), \quad (43b)$$

where  $\phi(z,t) = \int_0^z k(z') dz' - \omega t + \theta$ ,  $\phi_p(z,t) = \int_0^z \{k(z') + k_w(z')\} dz' - \omega t$  are the phases and the amplitudes of the potentials,  $A_R(z)$ ,  $\phi_1(z)$  and  $\phi_2(z)$  and the wavenumbers  $k(z)$  and  $k_w(z)$  are slowly varying functions of  $z$ . The scattered electromagnetic field represented by Eq. (43a) is a right-handed elliptically polarized field traveling in the positive  $z$  direction. The frequency  $\omega$  of the field and the phases as well as  $\theta$  are independent of  $z$ .

#### Wave Equations

The evolution of the scattered potentials are governed by the wave equations

$$\left( \frac{\partial^2}{\partial z^2} - \frac{1}{c^2} \frac{\partial^2}{\partial t^2} \right) \underline{A}_R(z,t) = - \frac{4\pi}{c} \underline{J}_1(z,t), \quad (44a)$$

and

$$\frac{\partial^2 \phi(z,t)}{\partial z \partial t} = 4\pi J_z(z,t), \quad (44b)$$

where  $J(z,t)$  is the driving current density. Substituting the potentials in Eqs. (43) into (44) yields

$$\{\omega^2/c^2 - k^2(z)\} A_R(z) \cos\phi(z,t)$$

$$-2k^{1/2}(z) \frac{\partial}{\partial z} \{A_R(z)k^{1/2}(z)\} \sin\phi(z,t) = -\frac{4\pi}{c} J_x(z,t), \quad (45a)$$

$$\frac{\partial}{\partial z} \{\phi_1(z)\sin\phi_p(z,t) - \phi_2(z)\cos\phi_p(z,t)\} = \frac{4\pi}{\omega} J_z(z,t), \quad (45b)$$

where terms proportional to  $\partial^2 A_R / \partial z^2$  have been neglected. The coefficients of the sinusoidal terms on the left-hand side of Eqs. (45) are slowly varying functions of  $z$  and independent of  $t$ . The arguments of the sinusoidal terms on the other hand are rapidly varying function of  $t$  for  $z$  fixed. The rapidly time-varying terms, in for example Eq. (45a), can be removed by multiplying them by  $\frac{\cos\phi(z,t)}{\sin\phi(z,t)}$  and taking the temporal average over one wave period, i.e.,  $(\omega/2\pi) \int_0^{2\pi/\omega} dt$ . Performing this operation on Eq. (45a) as well as similar operations on Eqs. (45b) yields

$$\{\omega^2/c^2 - k^2(z)\} A_R(z) = \frac{-4\omega}{c} \int_0^{2\pi/\omega} J_x(z,t) \cos\phi(z,t) dt, \quad (46a)$$

$$2k^{1/2}(z) \frac{\partial}{\partial z} \{A_R(z)k^{1/2}(z)\} = \frac{4\omega}{c} \int_0^{2\pi/\omega} J_x(z,t) \sin\phi(z,t) dt, \quad (46b)$$

$$\{k(z) + k_w(z)\} \phi_1(z) - \frac{\partial \phi_2(z)}{\partial z} = 4 \int_0^{2\pi/\omega} J_z(z,t) \cos\phi_p(z,t) dt, \quad (46c)$$

$$\{k(z) + k_w(z)\} \phi_2(z) + \frac{\partial \phi_1(z)}{\partial z} = 4 \int_0^{2\pi/\omega} J_z(z,t) \sin\phi_p(z,t) dt. \quad (46d)$$

### Nonlinear Driving Currents

It is now necessary to obtain expressions for the transverse and axial components of the current densities and perform the time integration specified

in Eqs. (46). In general the non-thermal electron distribution function, written in terms of the electron orbits, is

$$f(z, \underline{p}, t) = n_0 v_{z0} \int_{-\infty}^{\infty} \delta(z - \tilde{z}(t_0, t)) \delta(\underline{p} - \tilde{\underline{p}}(t_0, t)) \delta(p_y - \tilde{p}_y(t_0, t)) \delta(p_z - \tilde{p}_z(t_0, t)) dt_0 \quad (47)$$

where  $n_0$  is the uniform particle density to the left of the interaction region, i.e.,  $z < 0$ ,  $v_{z0}$  is the constant axial electron velocity for  $z < 0$ ,  $\tilde{z}(t_0, t)$  is the axial position of the particle at time  $t$  which crossed the  $z = 0$  plane at time  $t_0$  and  $\tilde{\underline{p}}(t_0, t)$  is the momentum vector of the particle at time  $t$  which crossed the  $z = 0$  plane at time  $t_0$ . Thermal effects which are characteristic of actual electron beams can be easily included by appropriately modifying the electron distribution function in (47). The integral over  $t_0$  in Eq. (47) takes into account the continuous flow of particles into the interaction region. The current density associated with this electron distribution is

$$\underline{J}(z, t) = \frac{-|e| n_0 v_{z0}}{m_0} \int_{-\infty}^{\infty} \frac{\underline{p}(t_0, t) \delta(t - \tau(t_0, z))}{\gamma(\underline{p}(t_0, t)) |\partial \tilde{z}(t_0, t) / \partial t|} dt_0, \quad (48)$$

where  $\gamma(\underline{p}) = (1 + |\underline{p}|^2 / m_0^2 c^2)^{1/2}$  and

$$\tau(t_0, z) = t_0 + \int_0^z \frac{dz'}{v_z(t_0, z')}, \quad (49)$$

is the time it takes a particle to reach the position  $z$  if it entered the interaction region,  $z = 0$ , at time  $t_0$  and  $v_z(t_0, z)$  is the axial velocity of a particle at position  $z$  which was at  $z = 0$  at time  $t_0$ .

The quantity  $\partial \tilde{z}(t_0, t) / \partial t$  is the axial velocity  $v_z$  of a particle at time  $t$  which was at  $z = 0$  at time  $t_0$ . Clearly, for  $J(z, t)$  to be finite,  $v_z$  should not vanish in the interaction region. We assume here that no particle is slowed down to zero velocity in the laboratory frame, hence

$\gamma(p(t_0, t)) m_0 |\partial \tilde{z}(t_0, t) / \partial t| = p_z(t_0, t)$  and the driving current becomes

$$J(z, t) = - |e| n_0 v_{z0} \int_{-\infty}^{\infty} \frac{p(t_0, t)}{p_z(t_0, t)} \delta(t - \tau(t_0, z)) dt_0. \quad (50)$$

Substituting the above form for  $J(z, t)$  into the right-hand side of Eqs. (46), we obtain the self-consistent amplitudes and phases of the scattered potentials in terms of driving currents.

Since the system of particles and fields are in the temporal steady-state, particles which cross the  $z = 0$  plane separated in time by  $2\pi/\omega$  will execute identical orbits which are separated in time by  $2\pi/\omega$ . It is, therefore, possible to define a beam segment, "beamlet", for which all possible steady-state orbits of the actual beam particles are represented by the particles in the beamlet, but are displaced in time. The axial length of the beamlet is clearly  $2\pi v_{z0}/\omega$ . Therefore, substituting (50) into (46) yields

$$\begin{aligned} & (\omega^2/c^2 - k^2(z)) A_R(z) \\ &= 4 |e| n_0 \frac{v_{z0}}{c} \omega \int_0^{2\pi/\omega} \frac{\tilde{p}_x(t_0, \tau(t_0, z))}{\tilde{p}_z(t_0, \tau(t_0, z))} \cos \phi(z, \tau(t_0, z)) dt_0, \end{aligned} \quad (51a)$$

$$\begin{aligned} & 2k^{1/2}(z) \frac{\partial}{\partial z} (A_R(z) k^{1/2}(z)) \\ &= - 4 |e| n_0 \frac{v_{z0}}{c} \omega \int_0^{2\pi/\omega} \frac{\tilde{p}_x(t_0, \tau(t_0, z))}{\tilde{p}_z(t_0, \tau(t_0, z))} \sin \phi(z, \tau(t_0, z)) dt_0, \end{aligned} \quad (51b)$$

$$\{k(z) + k_w(z)\}\phi_1(z) - \frac{\partial\phi_2(z)}{\partial z} = -4|e|n_0 v_{z0} \int_0^{2\pi/\omega} \cos\phi_p\{z, \tau(t_0, z)\} dt_0, \quad (51c)$$

$$\{k(z) + k_w(z)\}\phi_2(z) + \frac{\partial\phi_1(z)}{\partial z} = -4|e|n_0 v_{z0} \int_0^{2\pi/\omega} \sin\phi_p\{z, \tau(t_0, z)\} dt_0. \quad (51d)$$

Notice that on the right-hand side of the above equations the single integrals over  $t_0$  are from 0 to  $2\pi/\omega$ . As we will illustrate, these integrals can be evaluated numerically by following the orbits of a relatively small number of particles which enter the interaction region in any single time interval of duration  $2\pi/\omega$ .

### Particle Dynamics

We now express the particle orbits, which are needed for the evaluation of Eqs. (51) in terms of the new independent variables  $t_0$  and  $z$ . The forces exerted on the electrons arise from the wiggler and potentials given in Eqs. (41) and (43). We immediately note that the transverse canonical momenta of the particles is conserved. Therefore, if both the wiggler and scattered fields are zero as  $z \rightarrow -\infty$ , the transverse particle momenta are given by

$$p_x(z, t) = \frac{|e|\hbar}{c} (\underline{A}_w(z) + \underline{A}_R(z, t)) \cdot \hat{e}_x, \quad (52a)$$

and

$$p_y(z, t) = \frac{|e|\hbar}{c} (\underline{A}_w(z) + \underline{A}_R(z, t)) \cdot \hat{e}_y. \quad (52b)$$

Using Eqs. (52) the longitudinal component of the force equation can be put into the form

$$\frac{dp_z(z,t)}{dt} = \frac{-|e|^2}{2\gamma(z,t)m_0c^2} \left[ \frac{\partial}{\partial z} (A_w(z) + A_R(z,t))^2 - 2\gamma(z,t) \frac{m_0c^2}{|e|} \frac{\partial}{\partial z} \phi(z,t) \right], \quad (53)$$

where  $p_z(z,t)$  is the axial momentum and the relativistic mass factor is

$$\gamma(z,t) = \left[ 1 + \frac{|e|^2}{2m_0c^2} (A_w(z) + A_R(z,t))^2 + \frac{p_z^2(z,t)}{m_0^2c^2} \right]^{1/2}. \quad (54)$$

Equations (52) through (54) specify the particle dynamics in terms of the wiggler and scattered fields. The transverse and longitudinal particle motion is decoupled. Writing Eqs. (52) and (53) in terms of the new independent variables  $z$  and  $t_0$  we find that

$$p_x(z,\tau) = \frac{|e|}{c} (A_{wx}(z) + A_{Rx}(z,\tau)), \quad (55a)$$

$$p_y(z,\tau) = \frac{|e|}{c} (A_{wy}(z) + A_{Ry}(z,\tau)), \quad (55b)$$

$$\frac{dp_z(z,\tau)}{dz} = - \frac{|e|^2}{2c^2 p_z(z,\tau)} \left[ \frac{\partial}{\partial z} (A_w(z) + A_R(z,\tau))^2 - 2\gamma(z,\tau) \frac{m_0c^2}{|e|} \frac{\partial}{\partial z} \phi(z,\tau) \right]. \quad (55c)$$

We have expressed the particle orbits in terms of the entry time  $t_0$  and axial position  $z$ . Note that our definition of the momenta implies that,

$\tilde{p}_x(t_0,\tau) = p_x(z,\tau)$ ,  $\tilde{p}_y(t_0,\tau) = p_y(z,\tau)$ , and  $\tilde{p}_z(t_0,\tau) = p_z(z,\tau)$ . To obtain the final set of equations for the amplitude  $A_R(z)$  and wavenumber  $k(z)$  we first combine Eqs. (51a) and (51b) with Eqs. (51c) and (51d) respectively. Using the expressions for  $\tilde{p}_x$  and  $\tilde{p}_y$  given by Eqs. (55a,b) we arrive at the following expressions

$$(\omega^2/c^2 - k^2(z))A_R(z) = \frac{\omega_b^2}{2c^2} m_o v_{zo} \frac{\omega}{\pi} \int_0^{2\pi/\omega} \tilde{p}_z^{-1}(t_o, \tau(t_o, z))$$

$$\{A_w(z) \cos(\phi_p(z, \tau(t_o, z))) + A(z)\} dt_o. \quad (56a)$$

$$2k^{1/2}(z) \frac{\partial}{\partial z} (A_R(z) k^{1/2}(z)) = - \frac{\omega_b^2}{2c^2} m_o v_{zo} \frac{\omega}{\pi} \int_0^{2\pi/\omega} \tilde{p}_z^{-1}(t_o, \tau(t_o, z))$$

$$\{A_w(z) \sin(\phi_p(z, \tau(t_o, z)))\} dt_o, \quad (56b)$$

where we have used Eqs. (41) and (43a) for  $A_w(z)$  and  $A_R(z, t)$  and  $\omega_b = (4\pi|e|^2 n_o / m_o)^{1/2}$ . For completeness we rewrite Eqs. (51c) and (51d) for the scalar space charge potential

$$\begin{aligned} (k(z) + k_w(z))\phi_1(z) - \frac{\partial \phi_2(z)}{\partial z} \\ = \frac{-\omega_b^2}{c^2} \frac{v_{zo}}{\pi} \frac{m_o c^2}{|e|} \int_0^{2\pi/\omega} \cos(\phi_p(z, \tau(t_o, z))) dt_o, \end{aligned} \quad (57a)$$

$$\begin{aligned} (k(z) + k_w(z))\phi_2(z) + \frac{\partial \phi_1(z)}{\partial z} \\ = \frac{-\omega_b^2}{c^2} \frac{v_{zo}}{\pi} \frac{m_o c^2}{|e|} \int_0^{2\pi/\omega} \sin(\phi_p(z, \tau(t_o, z))) dt_o. \end{aligned} \quad (57b)$$

The relevant particle dynamics is contained in Eq. (55b) which is rewritten in the form

$$\frac{d\tilde{p}_z(t_o, \tau)}{dz} = \frac{-|e|^2}{c \tilde{p}_z(t_o, \tau)} \left[ \frac{\partial}{\partial z} (A_w(z) + A_R(z, \tau))^2 - 2\gamma(z, \tau) \frac{m_o c^2}{|e|} \frac{\partial \phi(z, \tau)}{\partial z} \right] \quad (58)$$

where

$$\gamma(z, \tau) = \left[ 1 + \frac{|e|^2}{2 m_0^2 c^4} |A_w(z) + A_R(z, \tau)|^2 + \frac{\tilde{p}_z(t_0, \tau)}{2 m_0^2 c^2} \right]^{1/2}, \quad (59a)$$

$$\tau(t_0, z) = t_0 + \int_0^z \frac{\gamma(z', \tau(t_0, z'))}{\tilde{p}_z(t_0, \tau(t_0, z'))} dz', \quad (59b)$$

$$\begin{aligned} |A_w(z) + A_R(z, \tau)|^2 &= A_w^2(z) + A_R^2(z) \\ &+ 2A_w(z)A_R(z)\cos\{\phi_p(z, \tau(t_0, z))\}. \end{aligned} \quad (59c)$$

The nonlinear formulation of the FEL is fully described by Eqs. (56), through (58). The ponderomotive potential plays a central role in axially bunching the electron. From Eq. (58) we see that this potential is given by

$$\phi_{\text{pond}}(z, \tau) = \frac{-|e|^2}{2 \gamma m_0 c^2} A_w(z)A_R(z) \cos\{\phi_p(z, \tau(t_0, z))\}. \quad (60)$$

The amplitude and phase of the scattered fields as well as the axial beam momentum all vary with a characteristic axial length which is much longer than the wiggler wavelength  $\lambda_w$ . This fact allows for inexpensive numerical simulations to be performed in the laboratory frame with extremely high energy electron beams.

#### Coupled Pendulum and Wave Equations

At this point our equations can be simplified and written in a more conventional form. To this end we define the electron's phase,  $\tilde{\psi}$ , with respect to the ponderomotive potential,

$$\tilde{\psi}(\psi_0, z) = \int_0^z (k(z') + k_w(z') - \omega/\tilde{v}_z(\psi_0, z)) dz' + \psi_0, \quad (61)$$

where  $\psi_0 = -\omega t_0$  is the electron's phase upon entering the interaction region at  $z = 0$  and  $\tilde{\psi}$  is also a function of the initial value  $\partial\tilde{\psi}/\partial z|_{z=0}$ . The second derivative of the electron's phase is

$$\frac{d^2\tilde{\psi}(\psi_0, z)}{dz^2} = \frac{d}{dz} (k_w + k) + \frac{\omega}{\tilde{v}_z^2(\psi_0, z)} \frac{d\tilde{v}_z(\psi_0, z)}{dz}. \quad (62)$$

Substituting (58) into (62) and assuming  $\gamma \gg 1$ ,  $|A_w| \gg |A_R|$  and  $v_z \approx \omega/(k + k_w) \approx c$  we find the following pendulum equation [29]

$$\begin{aligned} \frac{d^2\tilde{\psi}}{dz^2} = & \frac{d}{dz} (k_w + k) - \frac{|e|^2}{m_o^2 c^4} \frac{k_w}{\gamma_1^2} \frac{d}{dz} A_w^2 \\ & + \frac{4|e|^2}{m_o^2 c^4} \frac{k_w^2}{\gamma_1^2} [A_w A_R \sin\tilde{\psi} - \frac{\gamma m_o c^2}{|e|} (\phi_1 \sin\tilde{\psi} - \phi_2 \cos\tilde{\psi})], \end{aligned} \quad (63)$$

where  $\gamma_1 = (1 + (|e|A_w/m_o c)^2)^{1/2}$  is the relativistic mass factor associated with the transverse wiggler motion. In the absence of space charge effects, (63) reduces to the usual pendulum equation with a tapered wiggler [28] and without tapering [10]. Using the same assumptions as used to obtain the pendulum equation we find that

$$(\omega^2/c^2 - k^2(z))A_R(z) = \frac{\omega_b^2}{c^2} A_w(z) \left\langle \frac{\cos\tilde{\psi}(\psi_0, z)}{\gamma(z, \psi_0)} \right\rangle, \quad (64a)$$

$$k^{1/2}(z) \frac{d}{dz} (A_R(z) k^{1/2}(z)) = \frac{-\omega_b^2}{2c^2} A_w(z) \left\langle \frac{\sin\tilde{\psi}(\psi_0, z)}{\gamma(z, \psi_0)} \right\rangle, \quad (64b)$$

$$\phi_1(z) = \frac{2\omega_b^2}{\omega^2} \frac{m_o c^2}{|e|} \langle \cos \tilde{\psi}(\psi_o, z) \rangle, \quad (64c)$$

$$\phi_2(z) = \frac{2\omega_b^2}{\omega^2} \frac{m_o c^2}{|e|} \langle \sin \tilde{\psi}(\psi_o, z) \rangle, \quad (64d)$$

where  $\langle \dots \rangle = \int_0^{2\pi} (\dots) d\psi_o / 2\pi$  represents the ensemble average over the initial phases of the electrons. Equations (63) and (64) represent the full set of nonlinear equations describing the one dimensional FEL process with space charge effects and tapered wiggler.

### Numerical results in the Raman regime

In this section we present numerical results [27] for the coupled nonlinear FEL equations in (63) and (64). We assume that a monoenergetic electron beam enters the interaction region at  $z = 0$  with a uniform density. The magnetic wiggler field given in (41) is assumed to be built up adiabatically from  $z < 0$  to its initial value at  $z = 0$ . In all of our numerical simulations a small amplitude radiation field is introduced as a perturbation at  $z = 0$  and allowed to grow spatially and self-consistently according to the FEL equations.

We first consider the case where the magnetic wiggler parameters are fixed, i.e., constant amplitude and period. Later we consider the case where the wiggler period is adiabatically decreased, resulting in substantially higher radiation efficiency.

In this example submillimeter radiation at  $\lambda = 338 \mu\text{m}$  is generated using a 2.6 MeV electron beam. Table II lists the salient parameters for the wiggler field electron beam and output radiation. The magnetic wiggler amplitude 2.5 kG and the period is fixed at 2.0 cm. The 2.6 MeV ( $\gamma_o = 6$ ), 5 kA electron beam has a transverse equilibrium velocity of  $v_w = 0.078c$ .

Figure 5 shows the amplitude of the vector potential of the excited radiation,  $A_R(z)$ , and the spatial growth rate,  $\Gamma = \partial[\ln A_R(z)]/\partial z$ , as a function of  $z$ . These plots are for the frequency  $\omega = 2\gamma_{oz}^2 ck_w = 5 \times 10^{12} \text{ sec}^{-1}$  ( $\gamma = 338 \text{ } \mu\text{m}$ ). The long spatial region where the growth rate is fairly constant is the linear region of the interaction. The value of the radiation frequency in this figure has been chosen to maximize the linear growth rate. Figure 6 shows the amplitude of the beam space charge wave and the ponderomotive wave as a function of the interaction distance. Both wave amplitudes are of the same order of magnitude signifying that the process is for the most part in the Raman regime. Figure 7 shows the evolution of the wavenumber associated with the radiation field. Since the radiation wavenumber is greater than  $\omega/c$ , the effective index of refraction in the beam region is greater than unity. This implies that the radiation field will tend to focus inward towards the electron beam. Figure 8 shows a comparison between the linear growth rate obtained from the dispersion relation in (24) (solid curve) with the growth rate obtained from the linear regime of the fully nonlinear simulations (crosses (x)). Also in this figure the theoretical efficiency based on Eq. (35) (dashed curve) is compared with the nonlinear results (circles (o)).

#### Efficiency Enhancement

The phase velocity of the total longitudinal wave potential, i.e., ponderomotive plus space charge is approximately  $v_{ph} = \omega/(k + k_w)$ . The longitudinal wave potential is responsible for axially bunching and eventually trapping the electrons. If the wiggler period is held fixed, the radiation field reaches its maximum value when the electrons are trapped in the longitudinal potential wells. Just prior to the saturation of the

radiation field, the electrons are somewhat spatially bunched and trapped near the bottom of the wave potential. The trapped electrons at this point can be considered, for our purpose, to form a macro-particle. By appropriately reducing the phase velocity as a function of axial distance down the interaction region, the kinetic energy of this macro-particle can be further reduced and converted into wave energy. The phase velocity must be reduced in such a way so that the inertial potential of the trapped macro-particle is always less than the potential of the growing longitudinal wave. The phase velocity can be reduced by decreasing the period of the magnetic pump as a function of  $z$ . In order for the macro-particle to remain trapped, the spatial rate of change of the wiggler period must be sufficiently slow. In principle virtually all the kinetic energy of the macro-particle can be extracted and converted to wave energy. However, not all the beam particles comprise the macro-particle; some are untrapped. Converting particle kinetic energy into radiation by varying the wave velocity is somewhat analogous to the reverse process of particle acceleration in say an RF linac. Figure 9 illustrates the effect on the saturated radiation amplitude using a tapered wiggler field. In this figure the wiggler period is gradually decreased spatially at the point where the electrons are deeply trapped. Once the electrons are deeply trapped they are decelerated by decreasing the wiggler period [27,28]. Figure 9 demonstrates that dramatic enhancements in the FEL efficiency can be achieved in this way. (The parameters of Fig. 9 are different from Table II, and they are given in Ref. [27].) There are of course other schemes for enhancing efficiency in the FEL. These include, for example, spatially decreasing the wiggler amplitude [26,28] and/or applying an axial accelerating force such as a D.C. electric field [30,31] to the trapped electrons.

As a concluding comment, concerning the rapid growth of the free electron laser concept, the theory has been extended to include axial magnetic fields [32,33] thermal effects [34], three-dimensional effects [35,36] and the nonlinear stability of the radiation field [37]. Also a number of FEL experiments are now underway or in the planning phase and numerous workshops and special journal issues on the subject have appeared [7,38-42].

#### Acknowledgments

This work is sponsored by DARPA under Contract 3817.

Table I

The quantities used in Table I have the following definitions:  $\nu = I/17$  is Budker's parameter,  $I$  is the beam current in kiloamperes,  $L$  is the wiggler length,  $r_b$  is the beam radius,  $\beta_w = v_w/c$ ,  $\gamma_{oz} = \gamma_o / (1 + \gamma_o^2 \beta_w^2)^{1/2}$ ,  $f(\theta) = \partial (\sin \theta / \theta)^2 / \partial \theta$ ,  $\theta = (1 - v_{oz}/v_{ph}) \tau \omega / 2$ ,  $\tau = L/v_{oz}$  is the electron's transit time and  $F$  is the filling factor, i.e., beam area/radiation area. (c.g.s. units are used unless otherwise stated)

FEL Operating Regimes	Gain or Growth Rate	Intrinsic Power Efficiency
High Gain-Compton (single-particle)	$2 F^{1/3} \left\{ \frac{\nu}{\gamma_o} \right\}^{1/3} \left( \frac{r_b}{\lambda_w} \right)^{1/3} \frac{\beta_w^{2/3}}{r_b}$	$0.18 \left\{ \frac{\nu}{\gamma_o} \right\}^{1/3} \left( \frac{\lambda_w \beta_w}{r_b} \right)^{2/3}$
Raman (collective, high gain)	$(\pi \gamma_{oz} F)^{1/2} (\nu / \gamma_o)^{1/4} \frac{\beta_w}{\sqrt{r_b \lambda_w}}$	$\frac{1}{\pi \gamma_z} \left\{ \frac{\nu}{\gamma_o} \right\}^{1/2} \frac{\lambda_w}{r_b}$
Compton (single-particle, low-gain)	$\pi F \frac{\nu}{\gamma_o} (\beta_w)^2 \frac{L^3}{r_b^2 \lambda_w} f(\theta)$	$\frac{1}{2} \frac{\lambda_w}{L}$

Table II  
Raman FEL in the Submillimeter Regime  
(Constant Magnetic Wiggler Parameters)

Magnetic Wiggler Parameters		
Wiggler Wavelength	$\lambda_w$	2.0 cm
Wiggler Amplitude	$B_w$	2.5 kG
Electron Beam Parameters		
Beam Energy	$E_o$	2.6 MeV( $\gamma_o = 6$ )
Beam Current	$I_b$	5 kA
Axial Gamma	$\gamma_{zo}$	5.4
Beam Radius	$r_b$	0.3 cm
Wiggle Velocity	$\beta_w$	0.078
Self Potential Energy Spread	$\Delta E/E_o$	4.9%
Output Radiation Parameters		
Radiation Wavelength	$\lambda$	338 $\mu\text{m}$
Linear e-folding length*	$L_e = 1/\Gamma$	5.3 cm
Efficiency*	$\eta$	9.2%
Radiation Power*	$P$	1.2 GW

\* At the maximum growth rate.

## References

1. H. Motz, J. Appl. Phys. 22, 527 (1951).
2. R. M. Phillips, IRE Trans. Electron Devices 7, 231 (1960).
3. P. Sprangle and T. Coffey, Physics Today, 37, 44 (1984).
4. N. M. Kroll and W. A. McMullin, Phys. Rev. A 17, 300 (1978).
5. P. Sprangle, R. A. Smith and V. L. Granatstein, Infrared and Millimeter Waves, Vol. 1, K. J. Button, ed. New York: Academic Press (1979) p. 279, and NRL Memorandum Report 3911 (1978).
6. A. A. Kolomenskii and A. N. Lebedev, Sov. J. Quantum Electron 8, 879 (1978).
7. Free-Electron Generators of Coherent Radiation, Physics of Quantum Electronics, Vol. 7, 8 and 9, S. F. Jacobs, H. S. Pilloff, M. Sargent III, M. O. Scully and R. Spitzer eds. (Addison-Wesley, 1980).
8. L. R. Elias, W. M. Fairbanks, J. M. J. Madey, H. A. Schwettman and T. I. Smith, Phys. Rev. Lett. 36, 717 (1976).
9. D. A. G. Deacon, L. R. Elias, J. M. J. Madey, G. J. Ramian, H. A. Schwettman and T. I. Smith, Phys. Rev. Lett. 38, 892 (1977).
10. W. B. Colson, Phys. Lett. 64A, 190 (1977).
11. A. Gover and A. Yariv, Appl. Phys. 16, 121 (1978).
12. T. C. Marshall, S. Talmadge and P. Efthimion, Appl. Phys. Lett. 31, 320 (1977).
13. D. B. McDermott, T. C. Marshall, R. K. Parker and V. L. Granatstein, Phys. Rev. Lett. 41, 1368 (1978).
14. S. H. Gold, W. M. Black, H. P. Freund, V. L. Granatstein, P. C. Efthimion and A. K. Kinkad, Proc. of Free Electron Generators of Coherent Radiation (C. A. Brau, S. F. Jacobs and M. O. Scully, eds.) p. 350 (1983).
15. R. E. Shefer and G. Bekefi, in ref. 7, Vol. 9, p. 703-726.

16. C. W. Roberson, J. A. Pasour, F. Mako, R. Lucey and P. Sprangle, Infrared and Millimeter Waves, Vol. 10 (K. J. Button, ed.) Chapter 7, p. 361 (1983).
17. J. A. Pasour, R. R. Lucey and C. W. Roberson, Proc. of Free Electron Generators of Coherent Radiation, p. 328 (1983).
18. T. J. Orzechowski, B. Anderson, W. M. Fawley, D. Hopkins, A. C. Paul, D. Prosnitz, E. T. Scharlemann, A. M. Sessler, J. Wurtele and S. Yarema, "Microwave Radiation from a High Gain Free Electron Laser Amplifier", submitted for publication in Phys. Rev. Lett.
19. P. Sprangle and V. L. Granatstein, Appl. Phys. Lett. 25, 377 (1974).
20. A. T. Lin and J. M. Dawson, Phys. Fluids 18, 201 (1975).
21. J. M. J. Madey, Free Electron Generation of Extreme Ultraviolet Coherent Radiation, AIP Conf. Proc. No. 118. (Ed by J. M. J. Madey and C. Pellegrini), p. 12 (1984).
22. R. Bonifacio, C. Pellegrini and L. M. Narducci, Free Electron Generation of Extreme Ultraviolet Coherent Radiation, AIP Conf. Proc. No. 118. (Ed by J. M. J. Madey and C. Pellegrini), p. 236 (1984).
23. C. M. Tang and P. Sprangle, Free Electron Generation of Extreme Ultraviolet Coherent Radiation, AIP Conf. Proc. No. 118. (Ed by J. M. J. Madey and C. Pellegrini), p. 131 (1984).
24. C. M. Tang and P. Sprangle, NRL Memorandum Report 4670 (1981).
25. J. M. J. Madey, J. Appl. Phys. 42, 1906 (1971).
26. A. T. Lin and J. M. Dawson, Phys. Rev. Lett. 42, 1670 (1979).
27. P. Sprangle, C. M. Tang and W. M. Manheimer, Phys. Rev. Lett. 43, 1932 (1979) and Phys. Rev. A 21, 302 (1980).
28. N. M. Kroll, P. L. Morton and M. N. Rosenbluth, IEEE J. Quant. Electron, QE-17, 1436 (1981).

29. Cha-Mei Tang and P. Sprangle, J. Appl. Phys. 52, 3448 (1981).
30. A. T. Lin, Phys. Fluids 24, 316 (1981).
31. P. Sprangle and C. M. Tang, AIAA Journal 19, 1164 (1981).
32. R. C. Davidson and H. S. Uhm, J. Appl. Phys. 53, 2910 (1982).
33. H. P. Freund and P. Sprangle, Phys. Rev. A 26, 2004 (1982).
34. L. F. Ibanez and S. Johnston, IEEE J. Quant. Electronics 19, 339 (1983).
35. P. Sprangle and C. M. Tang, Appl. Phys. Lett. 39, 677 (1981).
36. N. S. Ginzburg, N. F. Kovalev and N. Yu Ruov, Optics Comm. 46, 300 (1983).
37. N. M. Kroll and M. N. Rosenbluth, in Ref. 7, Vol. 7, p. 147 (1980).
38. IEEE Trans. Microwave Theory Tech. (special issue) MTT-25, No. 6 (1977).
39. IEEE J. Quant. Electronics, QE-17, a special issue on free-electron lasers (1981).
40. IEEE J. Quant. Electronics, QE-19, a special issue on free-electron lasers (1983).
41. Proceedings of the Bendor Free Electron Laser Conf., Journal de Physique 44, C1 (1983).
42. Free Electron Lasers, edited by S. Martellucci and Arthur N. Chester, Plenum Press, New York (1983).

## Figure Captions

Figure 1      Power vs. Wavelength

The power vs. wavelength of some representative high power coherent radiation sources are shown. The output from recently reported free electron laser sources are shown and the type of electron beam source used indicated. The visible FEL's utilizing storage ring electron beams, are at a power level below the scale of the graph.

Figure 2      Shows a typical FEL configuration employing a linearly polarized wiggler field

Figure 3      Dispersion diagram of the coupled beam space charge modes and electromagnetic mode. The Raman FEL instability occurs near the intersection between the negative energy beam mode and electromagnetic mode.

Figure 4      Spatial growth rate and intrinsic efficiency in the Raman and high gain Compton regimes as a function of the wiggle velocity/c.

Figure 5      Shows the evolution of the radiation field amplitude and the growth rate as a function of the interaction distance.

Figure 6      Shows the spatial evolution of the beam space charge wave and ponderomotive wave amplitude. This illustration is in the Raman regime.

Figure 7      Shows the spatial evolution of the radiation wavenumber, the range where  $k$  is constant is the linear regime. Since  $k > \omega/c$  the radiation field will focus inward towards the electron beam.

Figure 8      Shows the comparison between the linear growth rate obtained from the dispersion relation (solid curve) and that obtained from the simulations in the linear regime (crosses (x)). Also shown is the theoretical efficiency based on Eq. (35) (dashed curve) compared with the nonlinear simulations (circles (o)).

Figure 9      Shows the enhancement of the radiation field and efficiency by tapering the wiggler period.

# FEL ACCELERATOR TYPE

● PULSE-LINE-DIODE

■ INDUCTION LINAC

▲ r-f LINAC

↓ STORAGE RING

